

radicals generated from the enzymatic or auto-oxidation of dopamine and other sources, compromised mitochondrial energy metabolism resulting from an environmental molecule such as 1-methyl-4-phenyl-1,2,3,6-tetrahydropyridine (MPTP) or oxidative stress, excitatory amino acid toxicity, and calcium toxicity (20). Because GDNF is able to protect DA neurons against several different types of injury in animal models of Parkinson's disease (2), GDNF gene therapy is likely to protect diseased human neurons, regardless of the mechanism of degeneration involved.

REFERENCES AND NOTES

1. L.-F. H. Lin, D. H. Doherty, J. D. Lile, S. Bektesh, F. Collins, *Science* **260**, 1130 (1993).
2. K. D. Beck *et al.*, *Nature* **373**, 339 (1995); A. Tomac *et al.*, *ibid.*, p. 335; C. M. Kearns and D. M. Gash, *Brain Res.* **672**, 104 (1995); B. J. Hoffer *et al.*, *Neurosci. Lett.* **182**, 107 (1994); K. E. Bowenkamp *et al.*, *J. Comp. Neurol.* **355**, 479 (1995); D. M. Gash *et al.*, *Nature* **380**, 252 (1996); H. Sauer, C. Rosenblad, A. Bjorklund, *Proc. Natl. Acad. Sci. U.S.A.* **92**, 8935 (1995).
3. DNA encoding human GDNF preproprotein (GenBank accession numbers L19062 and L19063) was synthesized by PCR with overlapping oligonucleotides. mGDNF, with deletion of amino acids 74 through 85 of mature GDNF, corresponding to nucleotides 300 through 335 of exon 2, was generated by PCR error. A black beetle virus translation enhancer element [Y. N. Chang, L. Y. Dong, G. S. Hayward, S. D. Hayward, *J. Virol.* **54**, 3358 (1990)] and Not I, Xba I, and Nde I restriction sites were included at the 5' end; Sal I, Bgl II and Cla I sites were included at the 3' end. Human GDNF and mGDNF DNAs were ligated into Xba I and Cla I sites in the Ad shuttle plasmid pAvS6 [T. A. G. Smith *et al.*, *Nature Genet.* **5**, 397 (1993)]. lacZ DNA with an NH₂-terminal SV40 large T antigen nuclear localization signal was also cloned into pAvS6. Transgenes were under the control of the RSV long terminal repeat promoter and were followed by an SV40 polyadenylation signal. Plasmids were cotransfected into 293 cells with the large fragment of Cla I-digested adenovirus serotype 5 genome dl327, and homologous recombination yielded Ad vectors with E1a and E3 (1.9-kb) deletions. Positive plaques were plaque-purified twice, cesium chloride banded, and characterized by PCR and Xba I digestion. Infectious particle concentrations (or PFU) were determined by infection of 293 cells, and total particle concentrations were determined by 260-nm absorbance. Viral stock titers (PFU per milliliter) and particle ratios (total particles per PFU) were as follows: Ad GDNF, 4×10^{10} , 30; Ad mGDNF, 4×10^{10} , 35; Ad lacZ, 2×10^{10} , 50.
4. L. A. Greene and A. S. Tischler, *Proc. Natl. Acad. Sci. U.S.A.* **73**, 2424 (1976).
5. Capture antibody [monoclonal antibody to human GDNF (3 μ g/ml) (R&D Systems, Minneapolis, MN)] was coated onto 96-well plates overnight at 4°C in phosphate-buffered saline (PBS). Wells were blocked with 1% bovine serum albumin (BSA) in PBS for 4 hours at room temperature (RT). Samples [50 μ l of CM or serial dilutions of recombinant human GDNF (R&D Systems)] were incubated overnight at 4°C. Detection of bound GDNF was by polyclonal antibody to human GDNF (2 μ g/ml), incubated overnight at 4°C, followed by horseradish peroxidase-coupled secondary antibody (0.4 μ g/ml) for 4 hours at RT; 0.02% ABTS [2, 2'-azino-bis(3-ethylbenzothiazoline)-6 sulfonic acid diammonium salt (Boehringer Mannheim, Indianapolis, IN)] and 0.03% H₂O₂ in 0.01 M sodium acetate, pH 5.0, were added and absorbance at 405 nm was measured.
6. J. Engele and M. C. Bohn, *Dev. Biol.* **152**, 363 (1992).
7. H. Sauer and W. H. Oertel, *Neuroscience* **59**, 401 (1994).
8. Rats were housed in the University of Rochester School of Medicine and Dentistry vivarium and were treated in accordance with institutional and NIH guidelines. FG (0.2 μ l, 2% in 0.9% saline) was stereotactically injected bilaterally into striatae at 0.05 μ l/min at +1.0 mm anterior (AP), 3.0 mm lateral (ML), and -5.0 mm ventral (DV) to the bregma [G. Paxinos and C. Watson, *The Rat Brain in Stereotaxic Coordinates* (Academic Press, Sydney, Australia, ed. 2, 1986)]. Ad vectors (2 μ l, 1.6×10^7 PFU/ μ l in 20% sucrose in PBS) were injected unilaterally dorsal to the SN at 0.5 μ l/min at -5.3 mm AP, 1.8 mm ML, and -7.4 mm DV to the bregma. The needle was left in place for 5 min and withdrawn at 1 mm/min. 6-OHDA-HBr [16 μ g of free base in 2.8 μ l of ascorbic acid (0.2 mg/ml) in 0.9% saline] was injected unilaterally into the striatum at 0.5 μ l/min at the same coordinates as FG. Rats were perfused with 100 ml of 0.9% saline followed by 300 ml of 4% paraformaldehyde in 0.1 M phosphate buffer, pH 7.4. After post-fix and cryoprotection, coronal sections were processed for TH immunofluorescence or TH immunocytochemistry with 1:1000 TH antibody (Chemicon, Temecula, CA). In addition, Ad lacZ transgene expression was followed by histochemistry with X-Gal [C. Cepko, in *Molecular Neurobiological Techniques*, A. A. Boulton, G. B. Baker, A. T. Campagnoni, Eds., vol. 16 of *Neuromethods*, A. A. Boulton and G. B. Baker, Eds. (Humana, Clifton, NJ, 1990), pp. 177-219].
9. D. L. Choi-Lundberg *et al.*, data not shown.
10. D. N. Angelov, A. Gunkel, E. Stennert, W. F. Neiss, *Glia* **13**, 113 (1995); L. Rinaman, C. E. Milligan, P. Levitt, *Neuroscience* **44**, 765 (1991).
11. Rats were injected with FG, Ad vector, and 6-OHDA (β), then killed by CO₂ suffocation. The ventral mesencephalon was dissected and frozen in liquid N₂. Tissue was sonicated in nine volumes of PBS, 0.1% Tween-20, 0.5% BSA, 2 mM EDTA, and protease inhibitors, then centrifuged at 40,000g for 12 min. The supernatant was used for GDNF (5) and β -Gal ELISA (5 Prime \rightarrow 3 Prime, Boulder, CO), and RNA and DNA were isolated from the pellet with Tri Reagent (Molecular Research Center, Cincinnati, OH).
12. P. Durbec *et al.*, *Nature* **381**, 789 (1996); S. Jing *et al.*, *Cell* **85**, 1113 (1996).
13. J. J. S. Treanor *et al.*, *Nature* **382**, 80 (1996); M. Trupp *et al.*, *ibid.* **381**, 785 (1996).
14. E. Arenas, M. Trupp, P. Akerud, C. F. Ibanez, *Neuron* **15**, 1465 (1995); A. Buj-Bello *et al.*, *ibid.*, p. 821; T. Ebendal, A. Tomac, B. J. Hoffer, L. Olson, *J. Neurosci. Res.* **40**, 276 (1995); C. E. Henderson *et al.*, *Science* **266**, 1062 (1994); H. T. J. Mount *et al.*, *Proc. Natl. Acad. Sci. U.S.A.* **92**, 9092 (1995); M. Trupp *et al.*, *J. Cell Biol.* **130**, 137 (1995).
15. D. L. Choi-Lundberg and M. C. Bohn, *Dev. Brain Res.* **85**, 80 (1995).
16. S. Akli *et al.*, *Nature Genet.* **3**, 224 (1993); G. Bajocchi, S. H. Feldman, R. G. Crystal, A. Mastrangeli, *ibid.*, p. 229; B. L. Davidson, E. D. Allen, K. F. Kozarsky, J. M. Wilson, B. J. Roessler, *ibid.*, p. 219; G. Le Gal La Salle *et al.*, *Science* **259**, 988 (1993).
17. A. P. Byrnes, J. E. Rusby, M. J. A. Wood, H. M. Charlton, *Neuroscience* **66**, 1015 (1995).
18. S. K. Tripathy, H. B. Black, E. Goldwasser, J. M. Leiden, *Nature Med.* **2**, 545 (1996).
19. Y. Yang *et al.*, *Nature Genet.* **7**, 362 (1994).
20. C. W. Olanow, *J. Neural Transm.* **91**, 161 (1993).
21. We thank R. Giuliano for assistance with cell culture, R. Anderson for assistance with preparation of viral stocks, J. Qian for neuropathological evaluation, and H. Federoff and W. Freed for their suggestions on the manuscript. Supported by NIH grants NS31957 (M.C.B.) and T32AG00107 (H.M.), the National Parkinson's Foundation, and Genetic Therapy, Inc.

3 June 1996; accepted 27 November 1996

Paradoxical Improvement of Impulse Conduction in Cardiac Tissue by Partial Cellular Uncoupling

Stephan Rohr,* Jan P. Kucera, Vladimir G. Fast, André G. Kléber

Generally, impulse propagation in cardiac tissue is assumed to be impaired by a reduction of intercellular electrical coupling or by the presence of structural discontinuities. Contrary to this notion, the spatially uniform reduction of electrical coupling induced successful conduction in discontinuous cardiac tissue structures exhibiting unidirectional conduction block. This seemingly paradoxical finding can be explained by a nonsymmetric effect of uncoupling on the current source and the current sink in the preparations used. It suggests that partial cellular uncoupling might prevent the initiation of cardiac arrhythmias that are dependent on the presence of unidirectional conduction block.

Cardiac tissue belongs to the broad class of reaction-diffusion systems that support excitation waves (1). In these systems, the

reduction of diffusion, which corresponds to uncoupling of gap junctions in the myocardium, is generally believed to impair wave propagation, promoting slow conduction, conduction block, and initiation of spiral waves (2). Disturbances of propagation can also be caused by structural discontinuities of the excitable medium, which correspond

Department of Physiology, University of Bern, Bühlplatz 5, CH-3012 Bern, Switzerland.

*To whom correspondence should be addressed. E-mail: rohr@pyl.unibe.ch

in the heart to discrete interconnections between muscle layers (3), to the Purkinje fiber ventricular junction (4), or to surviving tissue strands connecting islands of intact myocardial tissue in infarct scars (5). In all these structural discontinuities, a small current source is connected to a large current load, resulting in a current-to-load mismatch that causes slowing of conduction or conduction block. Both electrical uncoupling and the presence of discontinuous tissue structures are well known to be involved in the generation of life-threatening cardiac arrhythmias (6), and it is generally assumed that they act synergistically in the depression of conduction. Contrary to this assumption, the present study shows that uniform electrical uncoupling occurring in discontinuous tissue structures improves conduction.

Defined cardiac tissue geometries that exhibited, in a manner analogous to that of discontinuous tissue architectures in vivo, unidirectional conduction block due to a current-to-load mismatch were designed in cultures of neonatal rat ventricular myocytes with the use of photolithographic techniques (7). The preparations consisted of narrow cell strands ("strands") connected to rectangular cell monolayers ("expansions"; Fig. 1A) in which impulse propagation was followed by multiple site optical recording of transmembrane voltage (8). The mismatch between the size of the current source (strand) and the size of the current load (expansion) during anterograde activation (strand \rightarrow expansion) induced a conduction block if the strand width was $\leq 55 \mu\text{m}$. This block was due to the dissipation of depolarizing current from the strand into the expansion (9). In contrast, during retrograde propagation (expansion \rightarrow strand), when the source was much larger than the load, the entire preparation was rapidly activated. During the experiments, uncoupling of spatially defined regions of the preparations was achieved by placement of a microsuperfusion containing $10 \mu\text{M}$ palmitoleic acid over the region of interest (10). Palmitoleic acid, which has been found to accumulate in ischemic tissue (11), has previously been described as a potent uncoupler that does not affect action potential shapes in cultured heart cells of neonatal rats (12).

Initially, the isolated effects of uncoupling on either the current load or the current source were investigated. As shown in Fig. 1, uncoupling confined to the expansion induced successful anterograde conduction. Under control conditions (Fig. 1C), the anterograde conduction block due to the dissipation of depolarizing current into the expansion was mirrored by the decrement of signal amplitudes in the cell

strand close to the expansion. After superfusion of the expansion for 1.5 min with palmitoleic acid (Fig. 1D), the conduction block was overcome as indicated by the full depolarization of the entire preparation. Successful 1:1 conduction persisted for 2.5 min before the expansion became completely uncoupled and propagation came to an abrupt halt at the border of the superfusion (Fig. 1E). If a gradual uncoupling process due to the accumulation of palmitoleic acid in the cell membrane is assumed (12), this long period of successful conduction indicates that conversion of unidirectional conduction block occurred over a wide range of reduced gap-junctional conductances. During washout of palmitoleic acid, which was accompanied by progressive recoupling, the sequence was reversed as ac-

tivation captured increasingly larger areas of the expansion (Fig. 1, F and G) before successful anterograde conduction recurred after 4 min (Fig. 1H). After 10 min of washout, control conditions with anterograde conduction block were reestablished (Fig. 1I). Establishment of successful conduction during partial uncoupling of the expansion could be observed in all preparations tested ($n = 5$). In four of these preparations, activation invaded the expansion concentrically, which indicates a spatially uniform degree of uncoupling. In these cases, establishment of successful conduction is explained by the palmitoleic acid-induced increase of the internal resistance (r_i) of the expansion, which resulted in a homogeneous reduction of the load, thus leading to an improvement of the current-to-load mis-

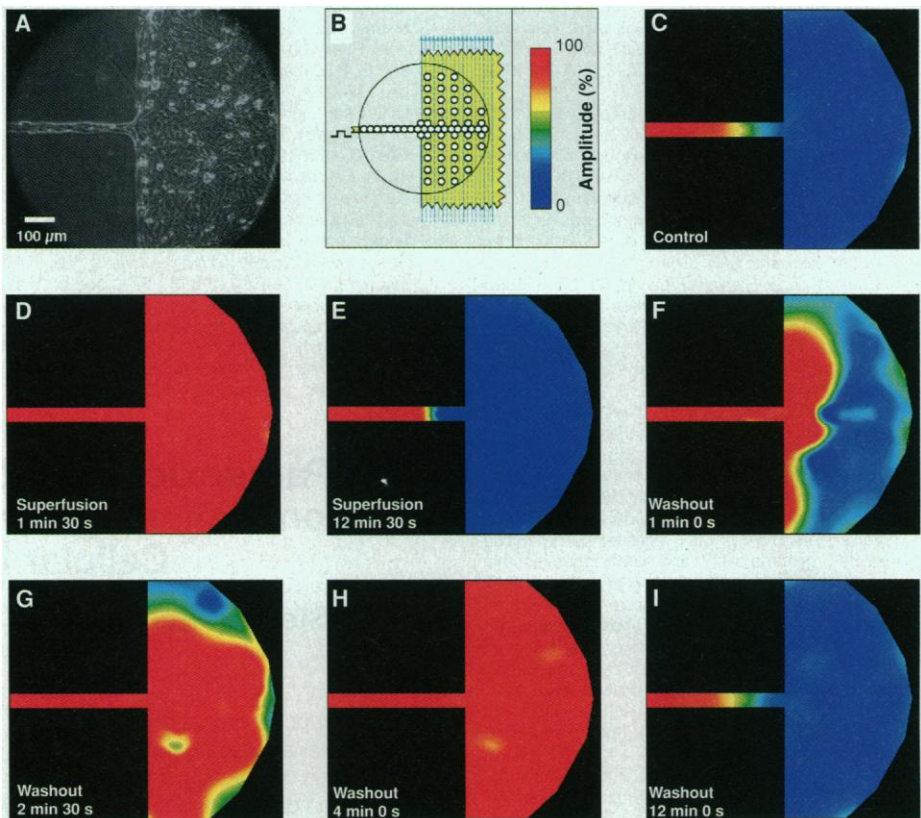


Fig. 1. Two-dimensional optical mapping of establishment of successful conduction across an abrupt tissue expansion during partial uncoupling of the expanding region. (A) Videomicrograph showing the patterned growth myocyte culture, which consisted of a narrow cell strand connected to a large rectangular cell monolayer (truncated to a semicircle by the field of view of the microscope). (B) Schematic drawing of the preparation (yellow) with overlaid white discs corresponding to the optical recording sites and a black circle indicating the field of view of the microscope. The preparation was stimulated in the anterograde direction at 2 Hz. The blue lines correspond to the region undergoing local superfusion with palmitoleic acid (width, $500 \mu\text{m}$). The false-color coding of the subsequent panels corresponds to maximal signal amplitudes reached during anterograde activation [red, full-sized action potentials; dark blue, absence of depolarization; for calculation see (8)]. Color maps were calculated from the discretely spaced recordings by quintic interpolation (16). (C) Under control conditions, the preparation exhibited anterograde conduction block. (D) During partial uncoupling of the expansion, successful anterograde activation was established. (E) After prolonged exposition to palmitoleic acid, the expansion became completely uncoupled. (F through H) With increasing washout time, activation captured increasingly larger areas of the expansion before invading the entire preparation. (I) After prolonged washout, unidirectional conduction block was reestablished.

match. In the remaining case, activation of the expansion followed a tortuous pathway suggesting that uncoupling was spatially nonuniform (13). In this case, the possibility cannot be excluded that, in addition to uncoupling, the formation of a funnel-like pathway of activation eased anterograde conduction across the abrupt expansion (9). In contrast to uncoupling of the expansion, partial uncoupling confined to the strand in front of the expansion failed, as expected, to initiate successful conduction ($n = 6$) (13). In these cases, the increase of r_i of the strand resulted in a reduction of the current source, thus aggravating the current-to-load mismatch.

The results of these experiments illustrated the isolated effects of uncoupling on the current source or the current load, but

cellular uncoupling occurring during disease *in vivo* will embrace entire discontinuous structures. In this situation, both the current source and the current load will be diminished. Because, in respect to the establishment of successful conduction, the effect of a reduction of the current source is opposite to a reduction of the current load, persistence of conduction block might be anticipated. Contrary to this expectation, the parallel uncoupling of the source and the load induced successful conduction as shown in Fig. 2. In this experiment, the local superfusion containing palmitoleic acid was placed so that it simultaneously affected the strand and the expansion (Fig. 2A). Under control conditions, anterograde conduction failed, as illustrated by the decrement in maximal signal amplitudes in the

cell strand due to the electrotonic interaction with the nonactivated expansion (Fig. 2B, left panel). At the same time, retrograde conduction was unhindered, as judged from the monophasically rising upstrokes of the action potentials (Fig. 2B, right panel) and the linear evolution of the activation times (Fig. 2B, middle panel). Six minutes of exposure to 10 μM palmitoleic acid induced bidirectional conduction block, with disruption of conduction coinciding with the borders of the superfusion (Fig. 2C). Then, during the washout-induced progressive recoupling, successful bidirectional conduction was established (Fig. 2D). After 10 min of washout, control conditions with unidirectional conduction block were restored (Fig. 2E). Establishment of successful anterograde conduction was observed in all preparations where the simultaneous uncoupling of both the strand and the expansion was induced by either a local superfusion ($n = 5$) or by adding palmitoleic acid directly to the bath solution ($n = 5$). With the exception of three experiments in which activation of the expansion followed a tortuous pathway, successful anterograde conduction was characterized by a concentric activation of the expansion, indicating a spatially uniform partial uncoupling. These results show that in discontinuous structures exhibiting unidirectional conduction block, uniform uncoupling embracing the entire tissue leads to successful bidirectional conduction. Thus, it has to be

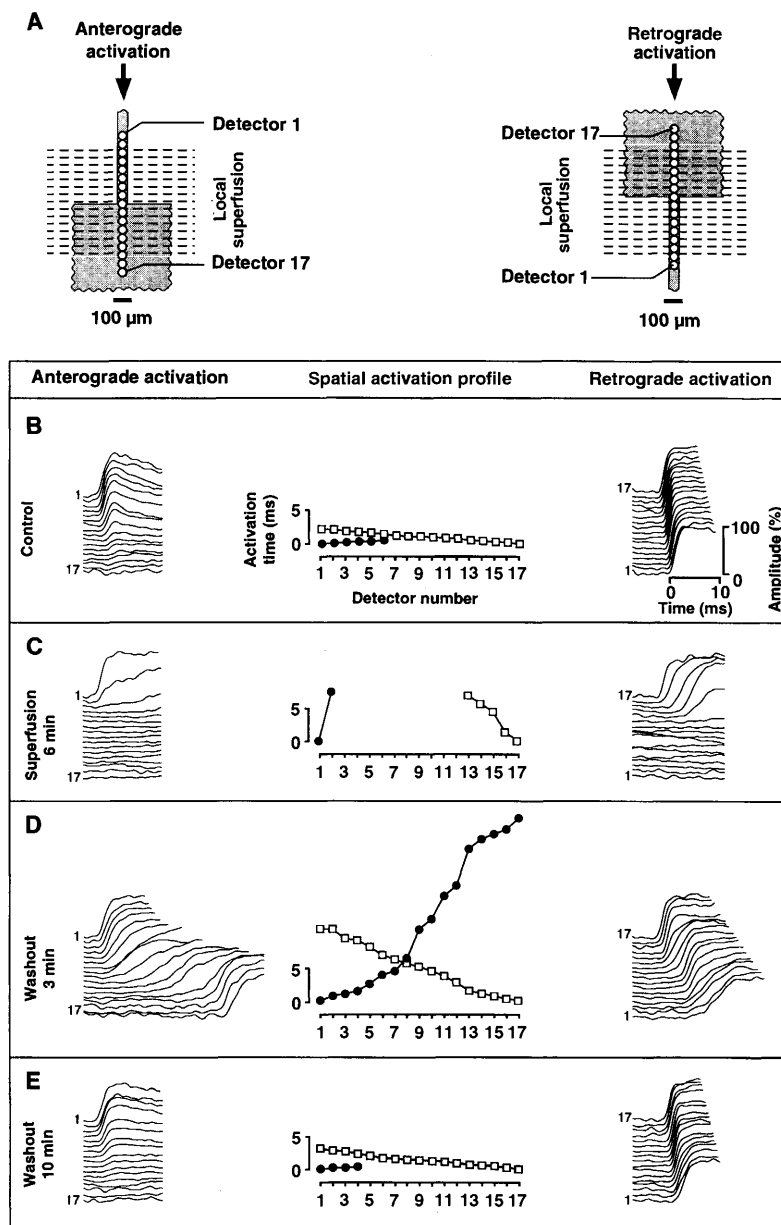


Fig. 2. Establishment of successful anterograde conduction across a tissue expansion during the simultaneous uncoupling of strand and expansion. (A) Schematic illustration of the experimental arrangement: Activation of the patterned growth preparation (gray) was recorded by 17 linearly arranged detectors (indicated by circles). The detector numbers correspond to the numbers associated with the signals in the subsequent panels. The preparation was stimulated alternately in the anterograde (left scheme) and retrograde (right scheme) direction at 2 Hz. The region marked with dashed lines corresponds to the area that was electrically uncoupled by a 700- μm -wide superfusion containing 10 μM palmitoleic acid. (B) Under control conditions, the preparation exhibited unidirectional conduction block in the anterograde direction (note the gradual reduction in signal amplitudes) and unhindered retrograde propagation (full-sized action potentials at all recording sites). Relative activation times for both directions of propagation are depicted in the center graph (solid circles, anterograde propagation; squares, retrograde propagation); their linear rise during retrograde propagation suggests that the preparation was homogeneously coupled. From this it can be inferred that unidirectional conduction block in the anterograde direction was entirely due to the current-to-load mismatch represented by the abrupt expansion. (C) After complete uncoupling of the center region of the preparation with 10 μM palmitoleic acid for 6 min, propagation was blocked in both directions with signal amplitudes decreasing to zero within a short distance (100 μm), coinciding with the borders of the superfusion. (D) During washout, successful bidirectional conduction was established with a large delay in the anterograde and a slowing of conduction in the retrograde direction. (E) After 10 min of washout, unidirectional conduction block was reestablished.

assumed that the effect of uncoupling on the load dominates over the effect of uncoupling on the source. This nonsymmetrical effect can be explained by local differences in the characteristics of depolarizing current flow in the strand versus the expansion: current flow in the strand is highly parallel, resulting in a planar activation wavefront, but it fans out into the expansion, giving rise to a curved activation wavefront. As suggested by recent computer simulations (14, 15), this difference in dimensionality of depolarizing current flow has the consequence that uncoupling has a smaller effect on the current source (reduction in one dimension) than on the current load (reduction in two dimensions), thus favoring the establishment of successful conduction. Even though the findings of this study are based on two-dimensional preparations, they are valid for three-dimensional tissue as well (15).

The results presented show that if a cellular network contains structural discontinuities, the modification of intercellular electrical coupling can have effects on impulse propagation that are largely different from those encountered in linear or continuous excitable structures. In general, the results show that a decrease of diffusion can support propagation of activation in discontinuous excitable media. For cardiac tissue, this might have the consequence that uncoupling, which is known to be involved in the generation of clinically relevant cardiac arrhythmias (6), might also exert anti-arrhythmic effects; even though cellular uncoupling induces an arrhythmogenic slowing of conduction, the possibility of a concurrent suppression of unidirectional conduction blocks in tissue regions with discontinuous structures would, contrary to present expectations, decrease the probability of occurrence of reentrant excitation.

REFERENCES AND NOTES

1. A. T. Winfree, *When Time Breaks Down* (Princeton Univ. Press, Princeton, NJ, 1987).
2. J. M. Davidenko, A. V. Pertsov, R. Salomonsz, W. Baxter, J. Jalife, *Nature* **355**, 349 (1992).
3. I. J. Le Grice *et al.*, *Am. J. Physiol.* **38**, H571 (1995).
4. R. D. Veenstra, R. W. Joyner, D. A. Rawling, *Circ. Res.* **54**, 500 (1984).
5. P. C. Ursell, P. I. Gardner, A. Albala, J. J. Fenoglio, A. L. Wit, *ibid.* **56**, 436 (1985); J. H. Smith, C. R. Green, N. S. Peters, S. Rothery, N. J. Severs, *Am. J. Pathol.* **139**, 801, (1991).
6. M. J. Janse and A. L. Wit, *Physiol. Rev.* **69**, 1049 (1989).
7. Geometrically defined patterns of cultured neonatal rat ventricular myocytes were obtained by means of a previously described method [S. Rohr, D. M. Schöllly, A. G. Kléber, *Circ. Res.* **68**, 114 (1991)]. The patterns used in the experiments consisted of cell strands (25 to 70 μm wide and 1.8 mm long) connected to a large rectangular cell monolayer (2.2 by 2.2 mm). The preparations were mounted on an inverted microscope equipped for epifluorescence and were superfused with Hank's balanced salt solution (pH 7.40 at 36°C).
8. The preparations were stained with the voltage-sensitive dye di-8-ANEPPS (Molecular Probes, Eugene,

OR), and propagating action potentials were elicited at a basic cycle length of 500 ms with extracellular stimulation electrodes at a distance of >1 mm from the recording area. Changes in transmembrane voltage were monitored with a system for multiple site optical recording of transmembrane voltage with a total of 80 detectors. Optically recorded signals at a given site were normalized to signal amplitudes measured at the same site during control retrograde propagation. If an average action potential amplitude of 100 mV is assumed, the values of these normalized signals translate directly into millivolts. Activation times were determined from the time when the signal at a given site reached 50% of the full amplitude [S. Rohr, *J. Cardiovasc. Electrophysiol.* **6**, 551 (1995)].

9. S. Rohr and B. M. Salzberg, *J. Gen. Physiol.* **104**, 287 (1994); V. G. Fast and A. G. Kléber, *Cardiovasc. Res.* **29**, 697 (1995).
10. The superfusion of defined regions of the preparation was performed with a system described elsewhere [J. Streit and H. D. Lux, *J. Neurosci.* **9**, 4190 (1989)]. The superfusion solution consisted of normal bath medium containing 10 μM palmitoleic

acid (dispersed by ultrasonication) and 20 mM sucrose, which rendered the superfusion visible through birefringence.

11. I. Miura, Y. Nasa, K. Ichihara, Y. Abiko, *Clin. Exp. Pharmacol. Physiol.* **18**, 259 (1991).
12. J. M. Burt, K. D. Massey, B. N. Minnich, *Am. J. Physiol.* **260**, C439 (1991).
13. S. Rohr, J. P. Kucera, V. G. Fast, A. G. Kléber, data not shown.
14. C. Cabo *et al.*, *Circ. Res.* **75**, 1014 (1994).
15. V. G. Fast and A. G. Kléber, *Cardiovasc. Res.* **30**, 449 (1995).
16. H. Akima, *Assoc. Comput. Mach. Trans. Math. Software* **4**, 148 (1978).
17. We thank R. Flückiger Labrada for preparing the heart cell cultures and H.-R. Lüscher, J. A. S. McGuigan, E. Niggli, A. L. Obaid, and J. S. Shiner for their helpful comments on the manuscript. Supported by the Swiss National Science Foundation and the Swiss Heart Foundation.

4 November 1996; accepted 3 December 1996

Calcium Waves in Retinal Glial Cells

Eric A. Newman* and Kathleen R. Zahs

Calcium signals were recorded from glial cells in acutely isolated rat retina to determine whether Ca^{2+} waves occur in glial cells of intact central nervous system tissue. Chemical (adenosine triphosphate), electrical, and mechanical stimulation of astrocytes initiated increases in the intracellular concentration of Ca^{2+} that propagated at ~ 23 micrometers per second through astrocytes and Müller cells as intercellular waves. The Ca^{2+} waves persisted in the absence of extracellular Ca^{2+} but were largely abolished by thapsigargin and intracellular heparin, indicating that Ca^{2+} was released from intracellular stores. The waves did not evoke changes in cell membrane potential but traveled synchronously in astrocytes and Müller cells, suggesting a functional linkage between these two types of glial cells. Such glial Ca^{2+} waves may constitute an extraneuronal signaling pathway in the central nervous system.

Glial cells, long considered to be passive elements in the central nervous system (CNS), are now known to generate active responses (1), including intracellular Ca^{2+} signals (2). Stimulation of astrocytes triggers increases in the intracellular Ca^{2+} concentration ($[\text{Ca}^{2+}]_i$) that can propagate as waves between cells coupled by gap junctions (3, 4). These glial Ca^{2+} waves have been observed only in dissociated cell (3–7) and organotypic (8) culture preparations, which differ from cells in situ in several respects (9). Because these waves may represent a form of intercellular signaling in the CNS (5) and can potentially modulate neuronal activity (10, 11), we tested whether Ca^{2+} waves occur in situ in glial cells of acutely isolated rat retina.

The rat retina contains two types of macroglial cells: astrocytes, which form a two-dimensional syncytium at the vitreal surface of the retina, and Müller cells,

which are radial glial cells whose end feet terminate at the vitreal surface and whose trunks project downward into the retina (12). We detected $[\text{Ca}^{2+}]_i$ in these cells with the fluorescent Ca^{2+} indicator dye Calcium Green-1 (13). The vitreal surfaces of flat-mounted retinas were imaged with video-rate confocal microscopy (14). Both astrocytes and Müller cells incorporated the dye and were identified by their morphology (Fig. 1A).

Stimulation of a single astrocyte evoked increases in $[\text{Ca}^{2+}]_i$ in the simulated cell and in neighboring astrocytes and Müller cells. This Ca^{2+} response propagated outward from the site of stimulation as a wave across the retinal surface (Fig. 1, B to D). Chemical, electrical, and mechanical stimuli were all effective in initiating Ca^{2+} waves. Pressure ejection of adenosine triphosphate (ATP) (200 μM), carbachol (1 mM), or phenylephrine (100 μM) from micropipettes onto astrocyte somata initiated Ca^{2+} waves. In contrast to findings in cultured cells (2, 5, 15), local ejection of glutamate (2 mM) or its application in the

Department of Physiology, University of Minnesota, 435 Delaware Street, SE, Minneapolis, MN 55455, USA.

* To whom correspondence should be addressed.